



High pressure hydrogen compression exploiting $\text{Ti}_{1.1}(\text{Cr,Mn,V})_2$ and $\text{Ti}_{1.1}(\text{Cr,Mn,V,Fe})_2$ alloys

Jussara Barale^{a,1}, Jose Ramón Ares^{b,*}, Paola Rizzi^a, Marcello Baricco^a,
Jose Francisco Fernandez Rios^b

^a Department of Chemistry and NIS - INSTM, University of Turin, Via Pietro Giuria 7, 10125 Torino, Italy

^b MIRE-Group, Department Física de Materiales, Facultad de Ciencias, Universidad Autónoma de Madrid, 28049 Madrid, Spain



ARTICLE INFO

Article history:

Received 21 November 2022

Received in revised form 20 February 2023

Accepted 28 February 2023

Available online 1 March 2023

Keywords:

Metal hydride compressor

Intermetallic Compound

AB_2 alloys

TiCrMn -based alloy

High pressure hydrogen compression

ABSTRACT

For metal hydride compressors to be used in substitution to the mechanical ones in the hydrogen infrastructures, it is mandatory to develop new compositions that can satisfy the desired goal of a pressure of 700 bar. To achieve the goal, Laves (C14) intermetallic compounds $\text{Ti}(\text{Cr,Mn})_2$ -based are very promising. New $\text{Ti}_{1.1}(\text{Cr,Mn,V})_2$ and $\text{Ti}_{1.1}(\text{Cr,Mn,V,Fe})_2$ compositions were synthesized and characterized in this work. The influence of the substitution of Cr with Mn and Fe on the crystal structure, and its correlation with the hydrogen sorption properties, was investigated, detecting an increment in the plateau pressure and the hysteresis gap. Thanks to suitable thermodynamics, developed alloys are good candidates for the high-pressure hydrogen compression. Moreover, they present an easy activation, that can be performed at room temperature, and a fast reaction rate, with few seconds required to absorb about 90% of the hydrogen content in the alloy. The most promising composition is the $\text{Ti}_{1.1}\text{Cr}_{0.9}\text{Mn}_{0.8}\text{V}_{0.1}\text{Fe}_{0.2}$, that is estimated to release hydrogen at about 700 bar at 150 °C. A possible integration of developed alloy in a metal hydride compressor is evaluated.

© 2023 The Authors. Published by Elsevier B.V. This is an open access article under the CC BY-NC-ND license (<http://creativecommons.org/licenses/by-nc-nd/4.0/>).

1. Introduction

The usefulness of hydrogen as compressed gas requires the achievement of high pressures, even higher than 700 bar, and its main application is related to the automotive or, more generally, the mobility sector [1]. So far, only mechanical compressors are able to satisfy the market demand, but they require a frequent maintenance and imply a high energy consumption, resulting in high costs of running and in being the main investment in a hydrogen refuelling station [2–4]. The use of metal hydride (MH) compressors as alternative to mechanical compressors was shown to be a promising technology. In fact, using MH, it is possible to compress hydrogen by a thermally driven mechanism of hydrogen sorption, resulting in an easy design, without requiring moving part, having low maintenance and limited costs of running [5,6].

Intermetallic compounds suitable for hydrogen sorption are based on an A metal, strongly interacting with hydrogen, and a B

metal, not forming hydrides, that can be described as AB (TiFe-type), AB_2 ($\text{Ti}(\text{Cr,Mn})_2$ -type) and AB_5 (LaNi_5 -type). After hydrogen absorption, by heating the formed MH, hydrogen is released at a higher pressure. The working temperatures, as named T_{low} for absorption and T_{high} for desorption, and pressures in absorption and desorption are defined by the equilibrium of the reversible reactions between the intermetallic compound and the hydrogen in forming the metal hydride, that are described in the pT-diagrams [5,6].

MH compressors available on the market can release hydrogen up to 250 bar working up to 150 °C [6–10]. To move toward a partial or total replacement of mechanical compressors, an extensive research activity is taking place out to find new compositions for intermetallic compounds that present an equilibrium pressure above 250 bar, possibly achieving up to 700 bar, operating at temperatures below 150 °C, or even lower than 100 °C, to allow the use of water for the heat management of the MH-reactors. Several new compositions of intermetallic compounds to be used in MH compressors at laboratory scale were developed in the past years, that can deliver H_2 at pressure above 350 bar, expecting the achievement of even 700 bar [11–23]. The AB_2 alloys with an hexagonal Laves phase (C14) are very promising for hydrogen compression purposes [24]. Both A and B elements can be easily substituted and an over- or under-stoichiometry can be also introduced, giving rise to a large number of compounds

* Corresponding author.

E-mail address: joser.ares@uam.es (J.R. Ares).

¹ Present Address: Tecnodelta S.r.l., Via Francesco Parigi 5H, 10034 Chivasso (To), Italy

with a wide range of properties [24]. In particular, compounds based on Ti, Cr and Mn, such as TiCr_2 , TiMn_2 and $\text{Ti}(\text{Cr,Mn})_2$, are very promising [6,8]. Depending on the relative amount of Cr and Mn, and on the substitution with other elements like V and/or Fe, compounds can display high plateau pressures at temperature even below 100 °C, making these alloys excellent candidates for applications in high pressure compressors [8,22,25–27]. However, small variations on the composition could have a great impact on the sorption properties. Properties that need to be taken into account when developing new compounds are also the activation and the occurrence of hysteresis. Indeed, activation is a pre-treatment necessary to facilitate the first H_2 absorption, that might be hindered by the presence of an oxide surface layer. The activation involves the processing of the material in temperatures and/or in pressures, promoting the cracking of the powder, and in turn the creation of new fresh surfaces to react, necessary to achieve a fast kinetics [28]. The conditions required for activation can change for different hydrides and also for the same compound, depending on its processing [29]. The occurrence of hysteresis implies that in isothermal conditions the absorption equilibrium pressure is higher than the desorption one. This is a complex phenomenon, that can depend on sample history (e.g. preparation conditions, microstructure) [30] and it is usually linked to a higher energy required by the hydrogen to overcome constraints generated by the increment of the volume of the hydride, compared to the parent intermetallic compound [31]. Finally, especially considering applications of hydrides in the market, important parameters are also the resistance to gas impurities and the stability over cycling, since they can cause a loss in hydrogen sorption properties, e.g. reducing kinetic properties and/or the storage capacity [28,32].

The AB_2 Ti-based binary alloys display two hydrides, i.e. $\text{TiX}_2\text{H}_{\sim 3}$ and $\text{TiX}_2\text{H}_{\sim 4}$ (X corresponding to a B-type metal), leading to two distinct plateaux in pC-T diagrams, but only for temperatures below 0 °C [33]. In ternary systems, by increasing the Mn content in $\text{TiCr}_{2-x}\text{Mn}_x$ with $0 \leq x \leq 1$, for $x > 0.75$, the absence of the $\text{TiX}_2\text{H}_{\sim 4}$ was observed [33]. In $\text{Ti}(\text{Cr,Mn})_2$ compounds, results from the literature suggest that increasing the Mn content, the hysteresis gap in pC-T diagrams is higher. On the other hand, the addition of V and Fe in substitution to Mn is beneficial in reducing it [22,34]. Hysteresis gap decreases also for compositions richer in Ti with respect to the stoichiometric compounds [35]. Compounds with over stoichiometry and/or substituted with V and/or Fe need milder activation conditions, if compared to the stoichiometric binary and ternary alloys [22,34,36]. The beneficial effect may be linked to surface and structural effects. In fact, the oxidation of the surface of the material due to the high affinity of Ti with oxygen might have a beneficial effect in hydrogenation, with the oxide phases acting as hydrogen channel promoting the activation of the matrix in mild conditions, as it was discussed for the $\text{TiFe}_{0.85}\text{Mn}_{0.05}$ in ref. [37].

Concerning the influence on the crystal structure, the over stoichiometry in Ti promotes an increase in cell parameters, thanks to the presence of Ti atoms also in Cr/Mn sites. The enlargement of the cell is due to the larger atomic radius of Ti compared to that of Cr/Mn. The rise in cell dimension causes a lowering in the equilibrium pressure [31]. The activation is enhanced also by the creation of vacancies in the Cr/Mn sublattice, which are promoted by the substitution in Cr/Mn site by Ti, that may act as a diffusion path for hydrogen atoms [38]. The change of the stoichiometry affects also the working conditions of pressure and temperature. Indeed, the enlargement of the cell occurs also with V that occupies both Cr/Mn and Ti site, while Fe, being slightly smaller than Cr, decreases cell dimensions [38]. The decreasing of the cell occurs also by increasing the Mn content, but not affecting the activation conditions [35]. The enlargement of the cell promoted by the increase of the Ti content was observed to be beneficial also in the storage capacity, with a value of 1.6 H_2 wt% observed for TiCrMn , to be compared with a value of 1.8 H_2 wt% for $\text{Ti}_{1.1}\text{CrMn}$ [35]. The increment in storage

capacity and the decrease of the hydrogen equilibrium pressure is strictly linked to the dimension of the interstitial sites. The larger are their dimensions, the lower is the energy required for hydrogen allocation, decreasing the pressure and increasing the storage capacity of the material [39,40]. Finally, the substitution of Cr and Mn with elements like V and Fe, affects the mechanical properties of the compounds, in terms of hardness, compared to the binary alloys [38], enhancing the cracking of the material during the activation, improving the hydrogenation.

Therefore, literature showed how minimal changes in the composition in the $\text{Ti}(\text{Cr,Mn,V,Fe})_2$ system can imply significant changes in the temperature and pressure working ranges and in activation conditions. Wang et al. [22] by preparing and studying a series of $\text{Ti}_{1+x}\text{Cr}_{2-y}(\text{Mn,V})_y$ alloys with $x = 0-0.2$ and $y = 0.4-0.8$, selected the $\text{Ti}_{1.2}\text{Cr}_{1.5}\text{Mn}_{0.4}\text{V}_{0.1}$ as second stage of a MH compressor, delivering H_2 at 450 bar at 170 °C, with an easy activation (conditions not given). In ref. [34], by studying $\text{TiCrMn}_{1-3x}\text{Fe}_{2x}\text{V}_x$, with $x = 0, 0.05, 0.1, 0.15$ and 0.2 , all the alloys, except the TiCrMn , were activated at about 150 bar and 20 °C. The $\text{TiCrMn}_{0.4}\text{Fe}_{0.4}\text{V}_{0.2}$ showed nearly no hysteresis, however the increase in Fe and V content promoted a significant decrease of the storage capacity by increasing the equilibrium temperature above 60 °C, leading to results that are not suitable for practical applications [34]. The optimal composition was suggested as $\text{TiCrMn}_{0.55}\text{Fe}_{0.30}\text{V}_{0.15}$ [34], that, integrated as 3rd stage in an MH compressor, was able to compress H_2 at 60 °C at 200 bar [41]. Finally, Boghilla and Niyas, in modelling a MH compressor to be integrated in a hydrogen refuelling station, investigated the use of $\text{Ti}_{1.1}\text{Cr}_{1.5}\text{Mn}_{0.4}\text{V}_{0.1}$, predicting an equilibrium of 350 bar at 150 °C [42]. In the light of previous works reported in the literature, it can be concluded that a promising composition based on these elements should contain an excess in Ti and a limited content of V and Fe, in order to have an easy activation, to maintain the high storage capacity of TiMn_2 and TiCr_2 , i.e. about 2.0 H_2 wt%, and to avoid a sensitive decrease of the operative temperatures. The Cr/Mn ratio has to be optimized, because it plays a crucial role on the hysteresis and equilibrium pressures.

In this work, starting from literature considerations, five $\text{A}_{1.1}\text{B}_2$ Laves (C14) new compositions based on Ti, Cr, Mn, V and Fe were synthesized, without performing any thermal treatment after the synthesis: $\text{Ti}_{1.1}\text{Cr}_{1.5}\text{Mn}_{0.4}\text{V}_{0.1}$ and $\text{Ti}_{1.1}\text{Cr}_{1.2}\text{Mn}_{0.7}\text{V}_{0.1}$; $\text{Ti}_{1.1}\text{Cr}_{1.3}\text{Mn}_{0.4}\text{V}_{0.1}\text{Fe}_{0.2}$, $\text{Ti}_{1.1}\text{Cr}_{0.9}\text{Mn}_{0.8}\text{V}_{0.1}\text{Fe}_{0.2}$ and $\text{Ti}_{1.1}\text{Cr}_{0.7}\text{Mn}_{1.0}\text{V}_{0.1}\text{Fe}_{0.2}$. The goal is to investigate the effect of the ratio between Mn and Cr, comparing results obtained for $\text{Ti}_{1.1}(\text{Cr,Mn,V})_2$ and $\text{Ti}_{1.1}(\text{Cr,Mn,V,Fe})_2$ at a fixed composition of Fe and V ($\text{Fe}_{0.2}$ and $\text{V}_{0.1}$, according to the work of Hagström et al. [34]). The relationship between the chemical and structural properties of the alloys and the hydrogen sorption were investigated. The use of composition in over stoichiometry was evaluated, based on the work of Wang et al., on the composition $\text{Ti}_{1.2}\text{Cr}_{1.5}\text{Mn}_{0.4}\text{V}_{0.1}$ [22]. It was decided to consider the same composition in the B elements of ref. [22], decreasing the Ti content, to investigate a possible decrease of the temperature necessary to reach an equilibrium of 450 bar (i.e. < 170 °C). Among new compositions developed in this work, the goal is to identify a possible alloy to be used as 3rd stage in a MH compressor [43], in order to increase the actual delivery pressure of 250 bar at 150 °C. So, the target composition should release H_2 at pressure ≥ 250 bar, with a $T_{\text{high}} \leq 150$ °C, evaluating if it is possible to even decrease the working temperature of the plant below 150 °C, to improve the plant thermal management and safety.

2. Experimental

Alloys were synthesized with arc melting starting from the parent elements commercialized by Alfa Aesar, with a purity of metals of Ti = 99.99%, Cr = 99.99%, Mn = 99.9%, V = 99.5% and Fe = 99.99%. The instrument by Edmund Bühler GmbH was used, working in Argon atmosphere (gas purity 5.5). Residual traces of

Table 1
Sample labels and the corresponding nominal chemical compositions.

Sample label	Chemical composition
Mn0.4	Ti _{1.1} Cr _{1.5} Mn _{0.4} V _{0.1}
Mn0.7	Ti _{1.1} Cr _{1.2} Mn _{0.7} V _{0.1}
FeMn0.4	Ti _{1.1} Cr _{1.3} Mn _{0.4} V _{0.1} Fe _{0.2}
FeMn0.8	Ti _{1.1} Cr _{0.9} Mn _{0.8} V _{0.1} Fe _{0.2}
FeMn1.0	Ti _{1.1} Cr _{0.7} Mn _{1.0} V _{0.1} Fe _{0.2}

oxygen in the chamber were removed by melting Ti and Zr getters. Compared to the nominal composition, synthesis involved a 5% and 2% weight excess of Mn and V, respectively, since they can evaporate during the melting process. About 13 g of alloy was prepared, by turning and melting the ingot about 5–7 times to homogenize the composition. Table 1 reports sample labels and the corresponding nominal compositions.

In the literature, Ti-Cr-Mn-based alloys are usually annealed at about 1000–1200 °C for a couple of days after the synthesis [34,36,44–46]. As mentioned in the introduction, in this work it was chosen to avoid any annealing. In fact, considering a possible large-scale production of developed alloys, thermal treatments cannot be easily performed at industrial level. In any case, some discrepancies between the prepared compositions at laboratory level and compositions prepared at industrial level can occur, due to a different purity of the starting elements [37]. Ingots were firstly manually broken in air and then manually grinded in Ar atmosphere inside a glovebox. The Ti_{1.1}Cr_{1.5}Mn_{0.4}V_{0.1} ingot, after being cooled with liquid nitrogen, was primary manually broken and then milled using a SPEX miller model 8000M for 5 min, since it was too hard to be manually grinded.

The particle size of the obtained powder was evaluated with a SEM instrument Hitachi S300 in Secondary Electron (SE) condition. A slice of the prepared ingots was embedded in a conductive resin and polished to investigate the microstructure and chemical composition by Scanning Electron Microscopy (SEM) in Back Scattered Electron (BSE) condition, coupled with Energy Dispersive X-ray (EDX), using the instrument Tescan Vega.

The structural study, aimed to define the phase fraction, were performed by acquiring Powder X-Ray Diffraction (PXD) patterns with the diffractometer X'Pert Pro in Bragg-Brentano geometry, equipped with a X'celerator detector and Cu-K α radiation. Analyses were performed on powdered sample before hydrogenation, acquiring patterns between 15° and 100° in 2 θ , step of 0.017° and time per scan of 400 s. A Rietveld refinement of diffraction patterns has been performed with the Maudsoftware [47].

Hydrogen sorption properties were investigated in a homemade volumetric apparatus built at the Universidad Autónoma de Madrid, equipped with a 3 stages metal hydride compressor [20]. Hydrogen (purity 6.0) was supplied up to 60 bar from a cylinder. When high pressure was required, it was compressed up to 140 bar by using the 3rd stage of the MH compressor at 140 °C [20]. About 0.80 g of sample were located in a stainless-steel reactor. Volumes have been calibrated, temperature and pressure at the sample were monitored as a function of time thanks to sensors, allowing the calculation of the amount of H₂ processed, the registration of absorption and desorption curves and the evaluation of the pcT-curves. Therefore, each point of the pcT-curves was taken evaluating a reasonable amount of H₂ to absorb/desorb to have a sufficient number of points. For pcT values in absorption, an error bar of 5% in H₂ wt% has been estimated, since the volumetric apparatus used is an homemade system and an instrumental error can occur, affecting in particular the last value due to the cumulative nature of the error. Temperature was controlled by an electric resistance and the sample can be cooled at temperatures lower than the room one, thanks to a water bath regulated by a chiller.

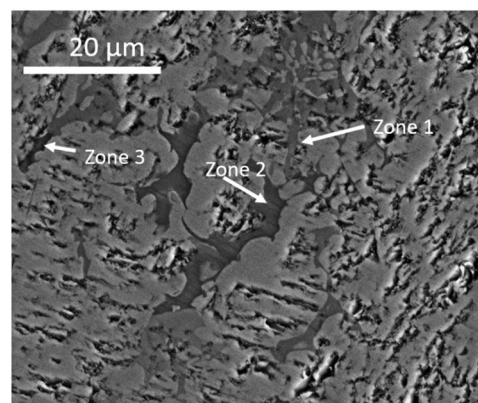


Fig. 1. SEM-BSE image acquired for sample FeMn0.8. White arrows highlight various greyscale zone compared to the matrix.

3. Results and discussion

3.1. Microstructure, composition, structure and morphology of the alloys

As an example, Fig. 1 shows the SEM-BSE image acquired for the sample FeMn0.8. Similar images for all other samples are shown in Fig. S1.

For all samples, together with the matrix, various zones with different greyscale are visible (white arrows), highlighting a non-homogeneous sample, as can be also deduced by results of the EDX elemental analysis, reported for each sample in Table S1. The latter reports the values of the matrix and of the various zones observed with the different greyscale. Numbers associated to the various zone indicate the progressive increase of the scale of grey, from the lightest to the darkest one, compared to the matrix, as it is shown in Fig. 1. In Table S1, it is also reported the stoichiometry calculated from the atomic elemental amount detected in the matrix, from which it is possible to see that the calculated stoichiometries are comparable to the nominal compositions reported in Table 1. From the chemical composition observed in different zones, in some cases oxygen was detected, suggesting the presence of some oxide phases (Table S1), visible in the SEM-BSE images as inclusions in the matrix or inside grain boundaries. The oxygen might be introduced during the synthesis from the raw materials and/or from alloy's processing. Zones detected without oxygen are mostly distributed among grain boundaries. These zones maintained an atomic ratio $Ti_{1.1}B_2$, as the matrix, but detecting a slightly different elemental amount compared to the matrix itself, e.g. in zone 2 and 3 of sample FeMn0.8 (Table S1). Only in sample Mn0.4, this phenomenon was not observed, and the zones 1 and 2 (Table S1) have an atomic ratio $Ti:B$ -elements close to 1:1. The latter atomic ratio was also detected in samples FeMn0.4 (zone 1 and 2) and FeMn1.0 (zone 4). Summarizing, the synthesis led to the formation of inhomogeneous samples and variations in the chemical compositions of the $A_{1.1}B_2$ were observed among grain boundaries, except in sample Mn0.4. An oxide phase was also detected in some samples, likely linked to the impurities in the raw materials or formed during sample preparation. Finally, zones with an atomic ratio close to AB_{-1} were also observed. Nevertheless, the oxides and the AB_{-1} zones were not detected in sample Mn0.7.

The crystal phases present in the synthesized samples were investigated by acquiring the PXD patterns, that are reported in Fig. 2.

PXD diffraction peaks related to the Laves (C14) phase are asymmetric and rather broad in all samples, except in sample Mn0.4. This phenomenon can be better visualized thanks to the use of red arrows in Fig. 2-f, comparing the diffraction peaks between 42° and 46° for sample FeMn0.8 (reported as an example of the others) and

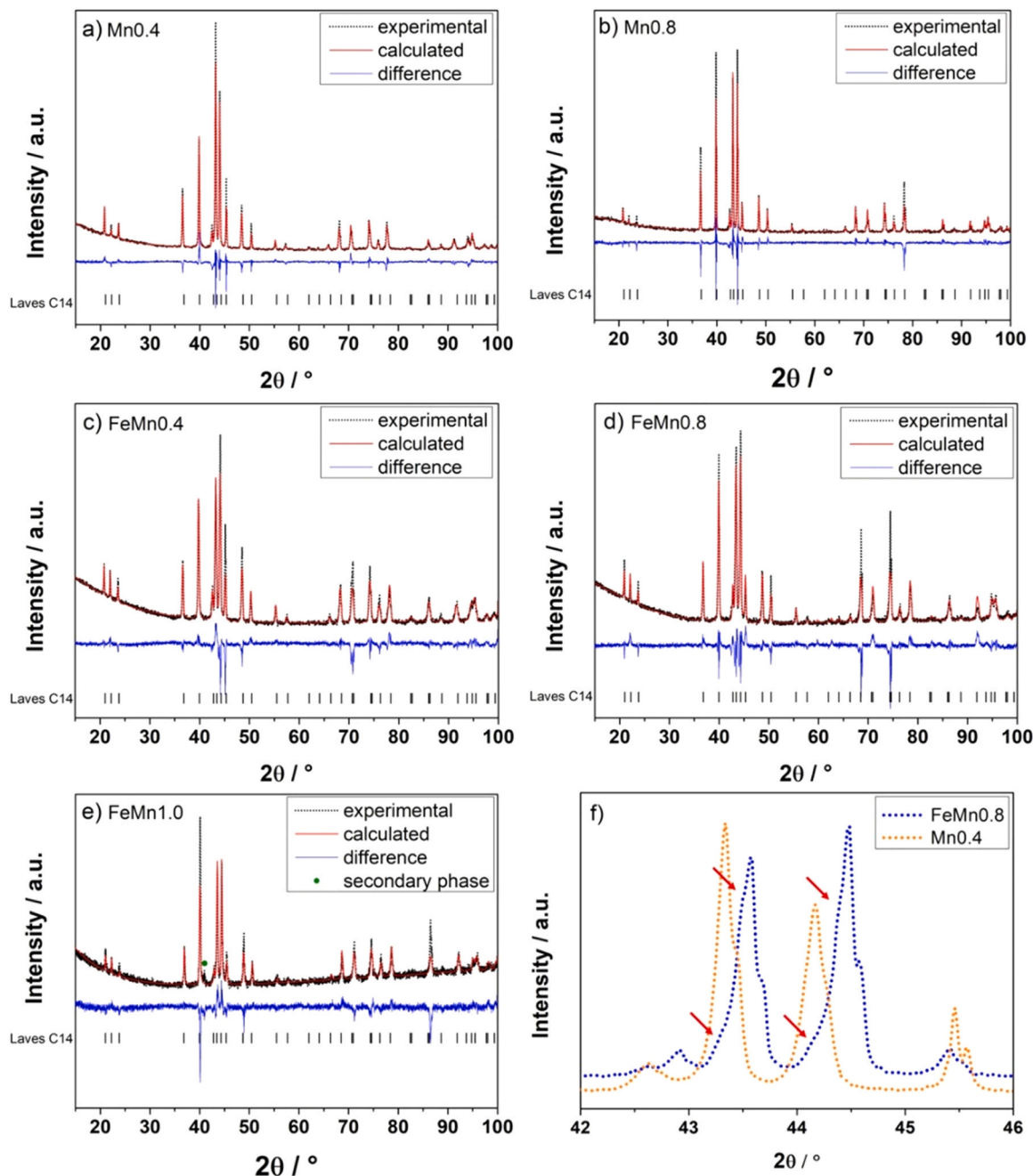


Fig. 2. Experimental and calculated from the Rietveld refinement PXD patterns, together with their differences, of samples: (a) Mn0.4; (b) Mn0.7; (c) FeMn0.4; (d) FeMn0.8; (e) FeMn1.0 in which the present of a secondary phase is highlight with a green circle; (f) zoom of the patterns for sample Mn0.4 and FeMn0.8 between 42° and 46° in 2θ , with red arrows to highlights the shoulders. Peak positions of the Laves phase C14 are reported as small bars.

Mn0.4. As previously reported from EDX results, only in Mn0.4 sample it was not detected the variation of the chemical composition from $A_{1.1}B_2$. Indeed, only one $A_{1.1}B_2$ composition was detected, and from the PXD pattern it has been linked to the Laves phase (C14). On the contrary, in all other samples (i.e. Mn0.7, FeMn0.4, FeMn0.8 and FeMn1.0), a chemical variation from the $A_{1.1}B_2$ stoichiometry was detected and diffraction peaks related to the Laves phase (C14) are broader with shoulders, if compared to those related to Mn0.4 sample. This observation suggests that, as it was already reported in ref. [48], the structure Laves phase (C14) is maintained for all the observed inhomogeneity of the composition of the $A_{1.1}B_2$. In the PXD pattern of sample FeMn1.0 reported in Fig. 2-e, the peak highlighted with a green circle is related to a secondary phase, likely corresponding to a $Ti_4(Cr,Mn,V,Fe)_4O$ oxide or to a TiMn-based phase, as

observed in the EDX analysis. The exact stoichiometry of the observed secondary phase is difficult to be assigned. On the other hand, in other patterns, no peaks due to secondary phases are visible. This results suggests that possible phases with stoichiometry AB_{-1} (FeMn0.4, Mn0.4) and the oxide (FeMn0.4, FeMn0.8) detected with the EDX are present in small amount, not being visible in the PXD patterns and, in turns, their role in the sorption properties could be neglected [48]. The Rietveld refinement was performed for all patterns considering only the Laves (C14) $A_{1.1}B_2$ phase, with the stoichiometry detected for the matrix. Finally, in sample FeMn1.0, the secondary phase was also excluded, due to the uncertainty on its structure. Table 2 reports the obtained cell parameters a and c for the Laves (C14) phase, together with the corresponding volume of the cell.

Table 2

Cell parameters *a* and *c* obtained from the Rietveld refinement of PXD patterns for all samples, together with the calculated volume of the cell.

Sample	Cell parameters / Å		Volume of the cell / Å ³
	<i>a</i>	<i>c</i>	
Mn0.4	4.908(6)	7.992(6)	166.722(9)
Mn0.7	4.875(7)	7.993(1)	164.509(0)
FeMn0.4	4.885(8)	8.003(9)	165.391(3)
FeMn0.8	4.869(2)	7.984(9)	163.919(5)
FeMn1.0	4.866(3)	7.977(9)	163.574(1)

As expected, Mn and Fe substitutions to Cr promote a decrease in cell parameters [38]. Comparing sample Mn0.4 with Mn0.7, the increase in the Mn content promotes the decrease in *a* cell parameter, while *c* values remain almost unaffected. Moreover, thanks to the substitution of Cr with Fe, the decrease is more remarkable, and it is evident also in *c* cell parameter, as can be seen comparing results obtained for sample Mn0.4 with FeMn0.4, i.e. compositions with the same amount of Mn. Afterwards, in the three samples containing Fe, the increase in Mn content promotes a decrease in cell dimension in both cell parameters *a* and *c*. In conclusion, as can be observed from Table 2, the cell volume decreases with the substitution of Cr with Mn and Fe, but it is not properly linked to a decrease of both cell parameters, as observed for the *c* and *a* cell parameters, comparing obtained values of samples Mn0.4 and FeMn0.4.

Fig. S2-a shows the SEM-SE image acquired for FeMn0.8 after the manual grinding, used as an example for all samples, while Fig. S2-b reports the image for Mn0.4 after milling. Powder's dimension was evaluated by the SEM-SE images. Due to the manual grinding, samples present a coarse particle size, as reported in the SEM-SE image for FeMn0.8 in Fig. S2-a. For samples containing Fe, the powder size is lower than 0.7 mm for FeMn1.0 and FeMn0.4 and lower than 0.5 mm for FeMn0.8. A slightly lower powder size was detected for sample Mn0.7 with a dimension lower than 0.2 mm. For the milled Mn0.4, as can be seen from the SEM-SE image reported in Fig. S2-b, a smaller dimension was obtained, observing powder agglomeration (zoom in Fig. S2-b) with a dimension of agglomerates lower than 0.3 mm.

3.2. Hydrogen sorption properties

3.2.1. Activation

The activation of (Ti,Zr)-(Cr,Mn,V,Fe)₂-based compounds is reported to occur at room temperature and in a pressure range lower than 150 bar [34,48]. Thus, for selected compounds, the activation in mild conditions, i.e. at room temperature and around 50 bar of H₂, was investigated.

The activation of all samples was reached at about 50 bar and room temperature (22 °C) in 2 cycles for Mn0.4, FeMn0.4 and FeMn1.0 compounds. The first cycle consisted of a hydrogen absorption for 2 h, followed by a desorption for 1 h, which occurred in a dead volume until a hydrogen pressure of 0.2 bar was reached and then followed by dynamic vacuum. The temperature profile linked to the hydrogen sorption in the first cycle of activation is reported in Fig. 3 as a function of time, and the corresponding hydrogen pressure profiles are reported in Fig. S3. Because the increment in temperature is linked to the exothermicity of the absorption of hydrogen by the sample, it is evident that as-prepared compounds are already reactive, easily absorbing H₂.

Comparing the curve of sample Mn0.4 with sample FeMn0.4, the absorption of hydrogen starts immediately after the supply of H₂ (Fig. S3), not observing any influence on the activation due to the Fe substitution. Moreover, no remarkable influence of particle size is observed into the H-kinetics absorption as Fig.S3 shows. On the contrary, Mn plays a role in activation, as can be observed by

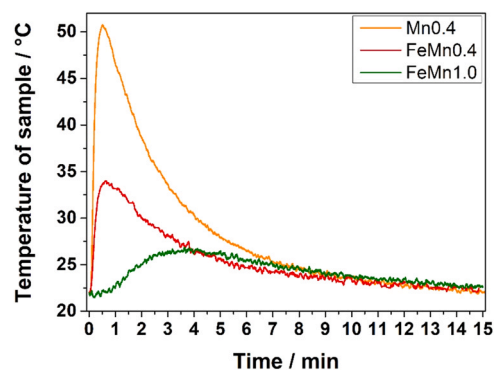


Fig. 3. Temperature profile of samples Mn0.4, FeMn0.4 and FeMn1.0 as a function of time acquired during the first cycle of activation during the absorption at room temperature under 50 bar of H₂.

comparing the temperature profile in sample FeMn0.4 with sample FeMn1.0. In fact, in the latter, the hydrogenation is still fast, but it starts after a longer incubation time. This phenomenon was not observed in sample FeMn0.8, that, on the contrary, presents a temperature profile similar to that of sample FeMn0.4, and so it has not been reported.

For sample Mn0.7, after the first cycle at 50 bar, in which no absorption was observed, two cycles at a hydrogen pressure of 120 bar were necessary to reach the activation. Higher temperature or pressure activation conditions by increasing the Mn content in AB₂ compounds were reported in the literature [35], linked to a decrease of the cell dimension and of interstitial sites. However, this effect is less remarkable with respect to the decrease of the cell dimension promoted by Ti [35,36]. Nevertheless, sample FeMn1.0 has still an easy activation, even if a higher content of Mn is present compared to sample Mn0.7, and also a lower cell volume (Table 2), so that 120 bar were necessary to succeed in the activation. From these observations, it seems that the higher pressure required for the activation is not strictly related to the Mn content in the composition. On the other hand, sample Mn0.7 is the only one in which secondary phases AB₂ or oxides were not detected (Table S1), while a certain amount of these phases is present in sample FeMn1.0, as observed in the PXD pattern (Fig. 2-e). So, the presence of secondary phases among grain boundaries is likely acting as H₂ diffusion path, promoting the cracking of the particles and, in turns, in enhancing the activation process. Thus, in sample FeMn1.0, the high fraction of secondary phase compensates the harder activation expected by the high Mn content in the composition. On the contrary, on sample Mn0.7, the absence of secondary phases required higher pressures compared to the other samples. Therefore, the secondary phases observed, even if present in a limited amount, can play a role in promoting the activation.

3.2.2. Thermodynamic characterization

For each sample, the pcT-curves were acquired for hydrogen absorption and desorption at 10 °C, 21 °C, 36 °C and 51 °C, and results are reported in Fig. S4. Expected plateaux are significantly sloped, likely due to samples inhomogeneity, as it was suggested in ref. [48]. The pcT-curves obtained for different samples are compared at 21 °C and 51 °C in Fig. 4. In detail, it shows the pcT-curves acquired for samples Mn0.4 and Mn0.7 at 21 °C (a) and 51 °C (b) and the pcT-curves of all the three samples containing Fe, i.e. FeMn0.4, FeMn0.8 and FeMn1.0, at 21 °C (c) and 51 °C (d). Fig. S5 shows again the pcT-curves of samples Mn0.4 and FeMn0.4 at 21 °C, to allow a better visualisation of the results between two compositions having the same amount of Mn, but a different content of Cr due to its substitution with Fe. In Fig. S4, Fig. S5 and Fig. 4, an error bar of the 5% in H₂ wt% has been added to the last value of pcT in absorption.

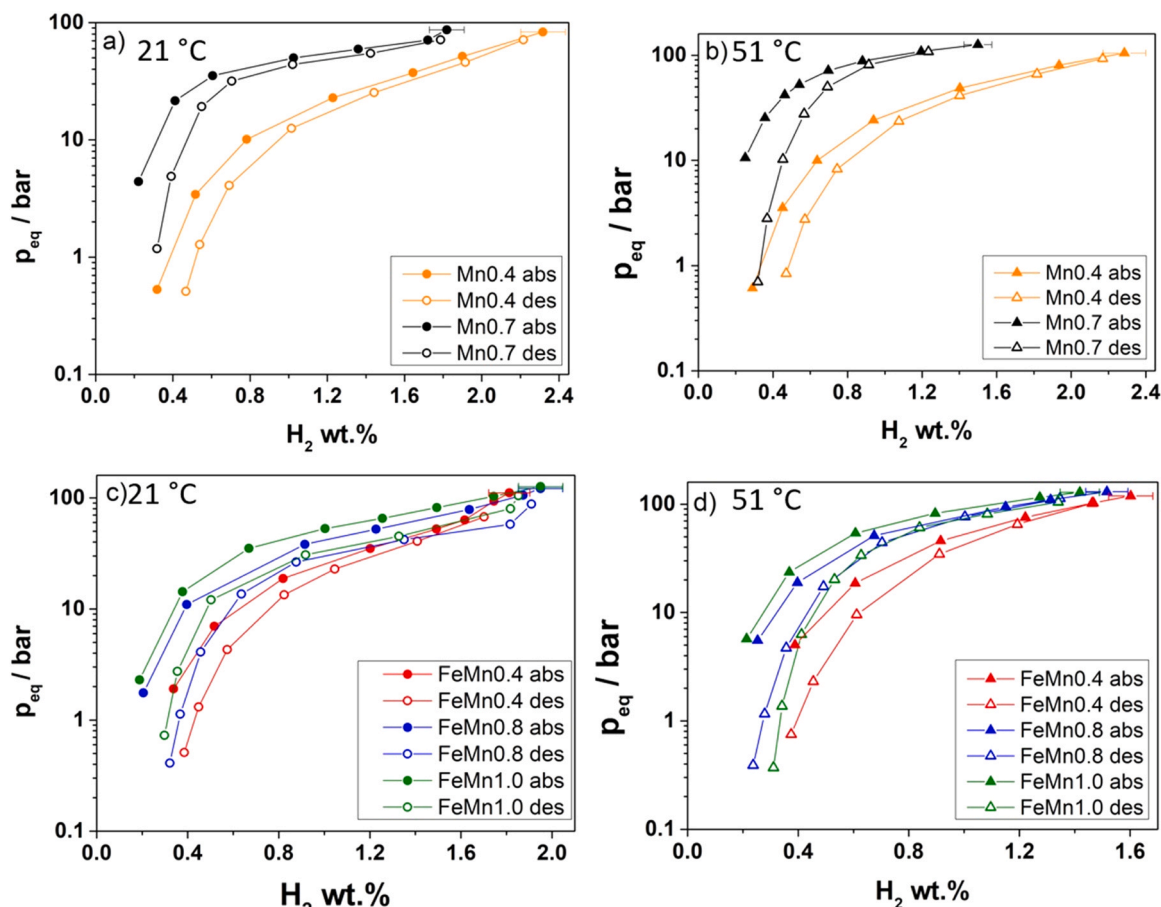


Fig. 4. pcT-curves in absorption (full points) and desorption (empty points): (a) samples Mn0.4 and Mn0.7 at 21 °C; (b) samples Mn0.4 and Mn0.7 at 51 °C; (c) samples FeMn0.4, FeMn0.8 and Mn1.0 at 21 °C (d) samples FeMn0.4, FeMn0.8 and Mn1.0 at 51 °C. An error bar of the 5% in H_2 wt% has been added to the last value in absorption.

As already mentioned, curves have sloping plateaux, and the slope increases with temperature, especially in samples containing Fe, as can be observed comparing pcT-curves at 21 °C and 51 °C (Fig. 4-c and d). By increasing the Mn content in samples $Ti_{1.1}(Cr,Mn,V)_2$ (Fig. 4-a, b), the equilibrium pressures in both absorption and desorption increase. While in samples $Ti_{1.1}(Cr,Mn,V,Fe)_2$ (Fig. 4-c, d), the absorption pressures increase with the Mn content, on the contrary of the desorption ones, registering comparable equilibrium pressures in desorption for sample FeMn0.8 and sample FeMn1.0. This is due to a substantial hysteresis gap in sample FeMn1.0, as can be seen from Fig. 4-c, d and Fig. S4. The hysteresis effect was quantified, from the observed absorption and desorption pressures (p_a , p_d) at 1.2 H_2 wt% at each temperature (T), as $R \cdot T \cdot \ln(p_a/p_d)$ [30]. It was detected that increasing the Mn content in the sample, the hysteresis increases from 21 J/mol for sample Mn0.4 up to about 116 J/mol for sample FeMn1.0. Finally, evaluating the substitution of Cr with Fe for a given content of Mn, comparing the pcT-curves of samples Mn0.4 and FeMn0.4 (Fig. S5), the equilibrium pressure in both absorption and desorption increases, linked to the decrease of the cell volume (Table 2). Finally, the H_2 storage capacity is maintained high, i.e. between 1.6 and 2.4 H_2 wt%.

Thermodynamic data for hydrogen absorption and desorption were evaluated between 1.0 and 1.6 H_2 wt%, depending on the sample. Corresponding Van't Hoff plots, with obtained values of enthalpy (ΔH) and entropy (ΔS), are reported in Fig. S6, together with the standard error of the linear fit obtained for a confidence level of 95%. The average values of the ΔH and ΔS in absorption and desorption are reported in Table 3, together with the corresponding error (Err.), evaluated as the propagation of the errors resulted from each linear fit, and the standard deviation of the average (Std. Dev.).

The propagated error on the average of the values reported in Table 3 as Err. was evaluated as the square root of the sum of the individual errors (E_i) squared and the whole divided for the number of the gravimetric capacities (N) considered for the average (Err.): $\sqrt{\sum E_i^2 / N}$.

In the series of $Ti_{1.1}(Cr,Mn,V,Fe)_2$ samples, since at least three samples can be considered, a linear fit was performed. Indeed, this linear correlation of the thermodynamic values states the presence of a compensation effect [49–51]. When this compensation effect occurs, ΔS and ΔH can be correlated according to Eq. (1):

$$\Delta H = \beta \Delta S + \text{const} \quad (1)$$

where β is the isoequilibrium temperature. This term represents the temperature at which all the systems considered react at the same rate [50]. This effect was observed in various reactions of different systems [51]. In our case, by plotting the obtained thermodynamic values, it can be observed that, in absorption, the linear correlation is associated with the rise in the Mn content in the compounds, while in desorption it does not. The evaluated isoequilibrium temperature, resulting by the linear fitting of the observed values, are 398 K in absorption and 239 K in desorption. Nevertheless, this thermodynamic and kinetic relation still lack for a full physical explanation [50]. In the literature, in case of reaction that involves the diffusion of atoms into metals (like in this case the diffusion of H atoms in the crystal structure), it has been suggested a linkage among the occurrence of the compensation effect, the presence of vacancies, the energy of the interstitial sites and, in turns, of the diffusion path [51].

Summarising, the decrease in cell volume due to the substitution of Cr with Mn and Fe promotes the increase of the equilibrium pressure for hydrogen absorption and desorption. However, in

Table 3

Values of enthalpy (ΔH) and entropy (ΔS), for hydrogen absorption and desorption, obtained from the Van't Hoff plots for each sample. The values are reported as the average of the values evaluated at different H_2 wt% together with the error obtained as propagation of the standards errors detected on each linear fit (Fig. S4) and the standard deviation of the average.

Sample	Absorption						Desorption					
	ΔH kJ/mol H_2			ΔS J/mol H_2 K			ΔH kJ/mol H_2			ΔS J/mol H_2 K		
	Av.	Err.	Std. Dev.	Av.	Err.	Std. Dev.	Av.	Err.	Std. Dev.	Av.	Err.	Std. Dev.
Mn0.4	14.14	0.40	0.68	75.71	1.33	2.07	13.34	0.21	0.63	71.81	0.71	3.17
Mn0.7	18.45	0.23	0.13	95.89	0.78	0.95	20.10	0.70	1.13	99.94	2.36	4.52
FeMn0.4	20.84	0.66	0.10	100.23	2.19	2.80	21.01	0.23	1.34	99.56	0.78	7.22
FeMn0.8	17.35	0.40	0.56	91.73	1.31	1.07	23.76	0.54	0.64	110.95	1.78	3.68
FeMn1.0	15.42	0.46	0.93	86.55	1.52	1.44	23.26	0.53	1.24	109.20	1.75	5.16

Values of ΔH are reported as a function of ΔS one in Fig. 5, considering the average values reported in Table 3. A certain linearity can be observed in both absorption and desorption.

sample FeMn1.0, the hysteresis gap is large, resulting in minimal advantage for compression purposes, for which the desorption thermodynamic properties determine the delivery pressure of the MH compressor. The desorption equilibrium pressure for all considered compounds was estimated from obtained thermodynamic data (Table 3) by extrapolation of the Van't Hoff relationship [5,42], considering as T_{high} , 100 °C, 120 °C and 150 °C, in order to estimate their individual performance as a potential 3rd stage for the MH compressor, as suggested in ref. [43]. A range of pressure is given in Table 3, since it has been taken into account the error on the values of ΔH and ΔS related to the linear fit of the Van't Hoff plot. Thus, this range of pressure includes the possible releasing hydrogen pressure from the MH compressor, linked to the uncertainty on the values of the thermodynamic data obtained from different values of gravimetric capacity in high sloped plateaux. The goal is to reach a delivery pressure ≥ 250 bar, i.e. higher than the delivery pressure of most of the MH compressor available in the market [6–10] and also higher than that reported in ref. [43]. The temperature of 100 °C was considered to evaluate the possibility to use water as thermal fluid. Then, 150 °C is considered because it is the actual working T_{high} of the MH compressor in ref. [43] and it is the working temperature of the commercially available MH compressors [6–10]. Finally, 120 °C was also evaluated as an intermediate temperature. Fig. 6 reports the obtained range of values of equilibrium pressure in desorption at the investigated T_{high} as a function of the volume of the cell evaluated for each sample (Table 2).

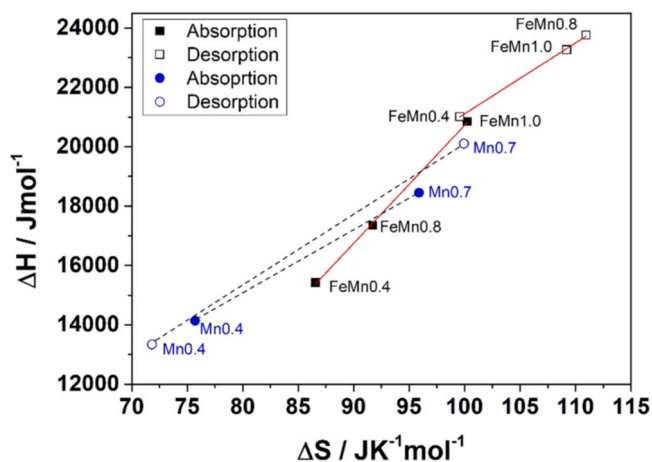


Fig. 5. ΔH values as a function of the ΔS ones for samples $Ti_{1.1}(Cr,Mn,V,Fe)_2$ in absorption (full black square points) and in desorption (empty black square points) are reported, together with the values of samples $Ti_{1.1}(Cr, Mn, V)_2$ in absorption (full blue circle points) and in desorption (empty blue circle points). The red line is the fitting line of the values linked to samples $Ti_{1.1}(Cr,Mn,V,Fe)_2$ Pearson's coefficient for the fitting in absorption is 0.99967, while in desorption is 0.99964. The connecting dashed lines for samples $Ti_{1.1}(Cr, Mn, V)_2$ are not linked to a linear fit, since only two values are available.

From Fig. 6, it can be observed that in samples FeMn1.0, FeMn0.8 and Mn0.7, i.e. in samples in which a large hysteresis and/or sloped plateaux have been detected in the pcT-curves (Fig. S4), a large range in the equilibrium pressure is obtained, compared to sample Mn0.4 and FeMn0.4. Thus, the lower is the hysteresis and the slope of the plateau, the limited is the error on the prediction of the equilibrium pressure, i.e. the error on the thermodynamic data obtained by extrapolation of the Van't Hoff plot.

Afterwards, sample Mn0.4 has a low range of p_{eq} (Fig. 6), even lower than 250 bar in all three investigated temperatures, so it would not be promising for high pressure applications. For this composition, $Ti_{1.1}Cr_{1.5}Mn_{0.4}V_{0.1}$, the equilibrium pressure observed in this work is lower than that reported in ref. [22,42]. This discrepancy can be linked to the different synthesis method used, confirming the sensitivity of the H_2 sorption properties on the material processing. Moreover, the comparison between the compound synthesised in this work and the one of ref. [22,42] is difficult, since only the performances observed by its integration in a MH compressor were reported, neglecting any chemical and structural characterisation.

Concerning other samples, thanks to the chemical substitutions and, as a consequence, the decrease in the cell volume, the estimated delivering pressure increases. The substitution of Cr with Fe, i.e. for sample FeMn0.4, allows already a remarkable increase in pressure, estimating a pressure higher than 250 bar already at 120 °C and achieving a maximum of about 416 bar at 150 °C. It can be noticed that a remarkable increase in pressure is achieved for the smallest cell volumes, i.e. for samples Mn0.7, FeMn0.8 and FeMn1.0. In fact, sample Mn0.7 might release hydrogen at about 250 bar already at

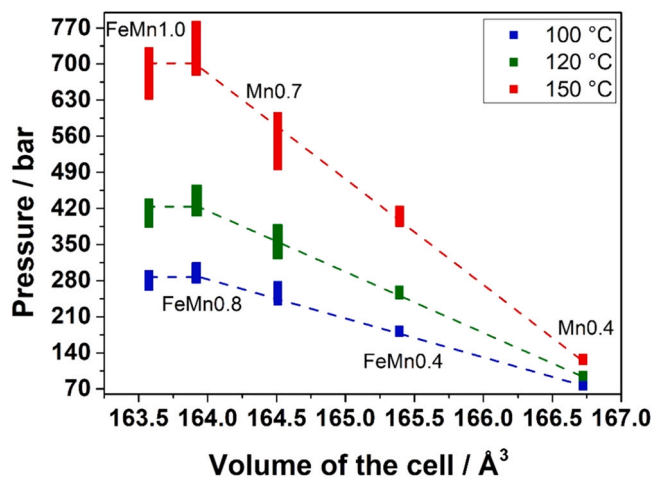


Fig. 6. Range of equilibrium pressures at different temperatures, obtained from thermodynamic data, as a function of the volume of the cell. Dashed lines are used as guidelines.

100 °C (range of 240 – 270 bar), estimating a pressure in the 331 – 380 bar range and in the 504 – 597 bar range at 120 °C and 150 °C, respectively. The possibility to increase the delivery pressure even above 300 bar is important, thinking to a possible commercial use and scaling up of the MH compressor. Indeed, if these types of alloys will be commercially available, their use in MH compressor is promising in hydrogen refuelling stations for the automotive sectors for buses or trains, where a pressure of 350 bar is required [1]. The highest values of pressure might be achieved in samples FeMn0.8 and FeMn1.0. Indeed, a range from 283 to 307 bar at 100 °C is estimated FeMn0.8, similar to the 269 – 292 bar range obtained for sample FeMn1.0. While at 150 °C, sample FeMn1.0 presents a 640 – 723 bar pressure range, close to the 686 – 776 bar estimated for sample FeMn0.8. Thus, due to the large hysteresis gap observed in FeMn1.0 from the pCT-curves (Fig. S4-e), might leads to a weak lowering of the equilibrium pressure in desorption compared to FeMn0.8.

In conclusion, the best composition among the five investigated for hydrogen compression results to be FeMn0.8 (Ti_{1.1}Cr_{0.9}Mn_{0.8}V_{0.1}Fe_{0.2}), in which a fast activation is observed, and a high desorption equilibrium pressure can be achieved.

3.2.3. Evaluation of selected alloy for a third stage of a MH compressor

According to results reported in Fig. 6 about the range of equilibrium pressure in desorption of Ti_{1.1}Cr_{0.9}Mn_{0.8}Fe_{0.2}V_{0.1}, working with a T_{high} between 100 °C and 150 °C, hydrogen can be released up to more than 700 bar. The MH compressor presented in ref. [43] involved the use of a La_{0.9}Ce_{0.1}Ni₅ alloy and the commercial Hydralloy-C5 as first and second stage, respectively. The T_{low} absorption temperature in the MH-beds was around 40 °C. Table 4 reports the estimated absorption and desorption equilibrium pressures involved in a possible three-stage MH compressor, based on the La_{0.9}Ce_{0.1}Ni₅, the Hydralloy-C5 and the Ti_{1.1}Cr_{0.9}Mn_{0.8}V_{0.1}Fe_{0.2} working at a T_{low} of 40 °C and a T_{high} of 100 °C, 120 °C and 150 °C. Reported pressures and temperatures take into account the working conditions registered during the tests performed on the MH compressor in ref. [43], and only an average value for output pressure is considered for Ti_{1.1}Cr_{0.9}Mn_{0.8}V_{0.1}Fe_{0.2} (Table 3).

For the considered values of T_{high}, the third stage might absorb H₂ from the Hydralloy-C5 only at 120 °C and 150 °C. In fact, at 100 °C the delivery pressure of the Hydralloy-C5 is equal to the absorption one of Ti_{1.1}Cr_{0.9}Mn_{0.8}V_{0.1}Fe_{0.2}. Thus, the results show that the three stages MH compressor might compress hydrogen from 16 to 436 or 729 bar, working between room temperature and 120 °C or 150 °C, resulting promising in real applications, if the Ti_{1.1}Cr_{0.9}Mn_{0.8}V_{0.1}Fe_{0.2} would be commercially available. Finally, for Ti_{1.1}Cr_{0.9}Mn_{0.8}Fe_{0.1}V_{0.1}, the transformed fraction, α , as a function of time, obtained absorbing H₂ at 11 °C at a supply pressure of 68 bar, is reported in Fig. 7.

It can be observed that a high reaction rate of the selected alloy is noted, with about 90% of the capacity reached in 50 s, implying few minutes to reach the full capacity. Same consideration can be made for the desorption of hydrogen. So, this alloy is promising for real scale applications, thanks also to its fast reaction rate.

Table 4

Absorption and deposition equilibrium pressure evaluated for a three stage MH compressor working at 40 °C of T_{low} and 100 °C, 120 °C and 150 °C of T_{high}.

	La _{0.9} Ce _{0.1} Ni ₅	Hydralloy-C5	Ti _{1.1} Cr _{0.9} Mn _{0.8} V _{0.1} Fe _{0.2}
T_{low}	P_{eq} absorption / bar		
40 °C	16	21	79
T_{high}	P_{eq} desorption / bar		
150 °C	130	200	729
120 °C	77	127	436
100 °C	46	80	295

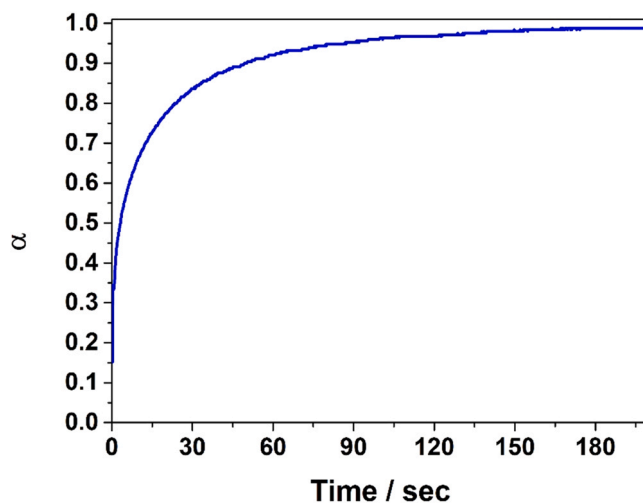


Fig. 7. The transformed fraction, α , for the hydrogenation at 11 °C and with a supply pressure of 68 bar of Ti_{1.1}Cr_{0.9}Mn_{0.8}Fe_{0.1}V_{0.1} compound as function of the reaction time.

4. Conclusions

Main conclusions can be summarized as follow.

- By investigating five AB₂ Laves (C14) compounds based on Ti, Cr, Mn, it was observed their potential use in hydrogen compression for high pressures. It was evidenced a crucial role of the structural and chemical composition on the sorption properties.
- By comparing results obtained in Ti_{1.1}Cr_{1.5}Mn_{0.4}V_{0.1} and Ti_{1.1}Cr_{1.2}Mn_{0.7}V_{0.1} alloys, the decrease in cell dimension, promoted by the substitution of Mn with Cr, implies a significant increase in the equilibrium pressure for both absorption and desorption. In Ti_{1.1}Cr_{1.2}Mn_{0.7}V_{0.1} compound, H₂ can be compressed at about 331–597 bar working between 120 °C and 150 °C, while a maximum of 130 bar could be reached with the sample Ti_{1.1}Cr_{1.5}Mn_{0.4}V_{0.1} at 150 °C. In the latter composition, by substituting Cr with Fe in Ti_{1.1}Cr_{1.3}Mn_{0.4}V_{0.1}Fe_{0.2}, a decrease in cell parameters was observed, resulting lower than that of Ti_{1.1}Cr_{1.5}Mn_{0.4}V_{0.1} compound, allowing to achieve a desorption pressure in the 251–262 bar range at 120 °C and 394–416 bar range at 150 °C. This result highlights how small changes in the composition can already have a high impact in the absorption and deposition equilibrium pressure.
- Maintaining the same Fe substitution, but changing the Cr/Mn ratio, in the Ti_{1.1}Cr_{0.9}Mn_{0.8}V_{0.1}Fe_{0.2} and in Ti_{1.1}Cr_{0.7}Mn_{1.0}V_{0.1}Fe_{0.2} compounds it was observed an almost linear decrease in cell parameters, coupled with an increment in the absorption pressure. However, a large hysteresis occurs in sample Ti_{1.1}Cr_{0.7}Mn_{1.0}V_{0.1}Fe_{0.2} resulting in a desorption pressure comparable to that observed in sample Ti_{1.1}Cr_{0.9}Mn_{0.8}V_{0.1}Fe_{0.2}, predicting a slightly higher delivery pressure in the latter sample.
- All the investigated samples can be activated easily in mild conditions with two hydrogen sorption cycles at 22 °C and 50 bar of hydrogen. The observed easy activation has been linked to the presence of a small amount of secondary phases, like AB₋₁ compound or oxide among grain boundaries. Indeed, a higher pressure of 120 bar was required for the activation of sample Ti_{1.1}Cr_{1.2}Mn_{0.7}V_{0.1}, in which no secondary phases were detected. Samples present also an inhomogeneity around the A₁B₂ composition, resulting in sloping plateaux.
- The Ti_{1.1}Cr_{0.9}Mn_{0.8}V_{0.1}Fe_{0.2} composition is very promising for real applications, thanks to high equilibrium pressure observed, implying the feasibility to achieve a pressure in the 283–307 bar

range at about 100 °C moving up to a 686–776 bar range at about 150 °C. In the studied conditions, the powder is already active and has a fast reaction rate.

This work highlights the extraordinary wide range of application of the Ti-Cr-Mn-V-(Fe)-based compounds, in which slight variations in the chemical composition can imply wide changes in the processing of hydrogen.

Finally, thanks to compounds properties and their potential in real life applications for the compression of hydrogen, future work should be devoted to investigate their stability over cycling and their resistance to gas impurities.

CRediT authorship contribution statement

J. Barale: Conceptualization, Investigation, Validation, Formal analysis, Writing – original draft, Visualization. **Jose Ramón Ares:** Resources, Conceptualization, Validation, Supervision, Writing – review & editing. **P. Rizzi:** Conceptualization, Supervision, Writing – review & editing. **M. Baricco:** Conceptualization, Supervision Writing – review & editing. **Jose Francisco Fernandez Rios:** Conceptualization, Investigation, Validation, Supervision, Writing – review & editing, Project administration.

Data availability

No data was used for the research described in the article.

Declaration of Competing Interest

The authors declare that they have no known competing financial interests or personal relationships that could have appeared to influence the work reported in this paper.

Acknowledgements

J.B. gratefully acknowledges the Erasmus+Traineeship programme 2020–2021 of the European Union for the financial support and for allowing the mobility between the University of Turin (Italy) and the Universidad Autonoma de Madrid (Spain) J.R.Ares and J.F. Fernández acknowledges the financial support of the Spanish MICINN under project RTI2018-099794-B-I00.

Appendix A. Supporting information

Supplementary data associated with this article can be found in the online version at [doi:10.1016/j.jallcom.2023.169497](https://doi.org/10.1016/j.jallcom.2023.169497).

References

- [1] J. Topler, J. Lehmann, *Hydrogen and Fuel Cell*, Springer, Berlin Heidelberg, 2016, <https://doi.org/10.1007/978-3-662-44972-1>
- [2] M. Lototsky, M.W. Davids, D. Swanepoel, G. Louw, Y. Klochko, F. Smith, F. Haji, I. Tolj, S. Chidziva, S. Pasupathi, V. Linkov, Hydrogen refuelling station with integrated metal hydride compressor: layout features and experience of three-year operation, *Int. J. Hydrog. Energy* 45 (2020) 5415–5429, <https://doi.org/10.1016/j.ijhydene.2019.05.133>
- [3] J.O. Jensen, A.P. Vestbø, Q. Li, N.J. Bjerrum, The energy efficiency of onboard hydrogen storage, *J. Alloy. Compd.* 446–447 (2007) 723–728, <https://doi.org/10.1016/j.jallcom.2007.04.051>
- [4] G. Sdanghi, G. Maranzana, A. Celzard, V. Fierro, Review of the current technologies and performances of hydrogen compression for stationary and automotive applications, *Renew. Sustain. Energy Rev.* 102 (2019) 150–170, <https://doi.org/10.1016/j.rser.2018.11.028>
- [5] M.V. Lototsky, V.A. Yartys, B.G. Pollet, R.C. Bowman, Metal hydride hydrogen compressors: a review, *Int. J. Hydrog. Energy* 39 (2014) 5818–5851, <https://doi.org/10.1016/j.ijhydene.2014.01.158>
- [6] J. Bellósta von Colbe, J.-R. Ares, J. Barale, M. Baricco, C. Buckley, G. Capurso, N. Gallandat, D.M. Grant, M.N. Guzik, I. Jacob, E.H. Jensen, T. Jensen, J. Jepsen, T. Klassen, M.V. Lototsky, K. Manickam, A. Montone, J. Puszkil, S. Sartori, D.A. Sheppard, A. Stuart, G. Walker, C.J. Webb, H. Yang, V. Yartys, A. Züttel, M. Dornheim, Application of hydrides in hydrogen storage and compression: achievements, outlook and perspectives, *Int. J. Hydrog. Energy* 44 (2019), <https://doi.org/10.1016/j.ijhydene.2019.01.104>
- [7] V.A. Yartys, M.V. Lototsky, V. Linkov, S. Pasupathi, M. Wafeeq, I. Tolj, G. Radica, R.V. Denys, J. Eriksen, K. Taube, J. Bellósta, V. Colbe, G. Capurso, M. Dornheim, F. Smith, D. Mathebula, D. Swanepoel, ScienceDirect HYDRIDEAMOBILITY: An EU HORIZON 2020 project on hydrogen powered fuel cell utility vehicles using metal hydrides in hydrogen storage and refuelling systems, *Int. J. Hydrog. Energy* (2021) 1–14, <https://doi.org/10.1016/j.ijhydene.2021.01.190>
- [8] V.A. Yartys, M. Lototsky, V. Linkov, D. Grant, A. Stuart, J. Eriksen, R. Denys, R.C. Bowman, D. Grant, A. Stuart, Metal hydride hydrogen compression: recent advances and future prospects, *Appl. Phys. A* 122 (2016) 1–18, <https://doi.org/10.1007/s00339-016-9863-7>
- [9] GRZ Technologies website, (n.d.), (<https://grz-technologies.com>).
- [10] HYSTORSYS SA website, (n.d.), (<http://www.hystorsys.no>).
- [11] F. Laurencelle, Z. Dehouche, J. Goyette, T.K. Bose, Integrated electrolyser-metal hydride compression system, *Int. J. Hydrog. Energy* 31 (2006) 762–768, <https://doi.org/10.1016/j.ijhydene.2005.06.019>
- [12] M. Visaria, I. Mudawar, Experimental investigation and theoretical modeling of dehydrogenation process in high-pressure metal hydride hydrogen storage systems, *Int. J. Hydrog. Energy* 37 (2012) 5735–5749, <https://doi.org/10.1016/j.ijhydene.2011.12.140>
- [13] X. Wang, H. Liu, H. Li, A 70 MPa hydrogen-compression system using metal hydrides, *Int. J. Hydrog. Energy* 36 (2011) 9079–9085, <https://doi.org/10.1016/j.ijhydene.2011.04.193>
- [14] V.V. Solovey, A.I. Ivanovsky, V.I. Kolosov, Y.F. Shmal'ko, Series of metal hydride high pressure hydrogen compressors, *J. Alloy. Compd.* 231 (1995) 903–906, [https://doi.org/10.1016/0925-8388\(95\)01780-1](https://doi.org/10.1016/0925-8388(95)01780-1)
- [15] D.B. Smith, R.C. Bowman, L.M. Anovitz, C. Corgnole, M. Sulic, Isotherm measurements of high-pressure metal hydrides for hydrogen compressors, *JPhys Energy* 3 (2021), <https://doi.org/10.1088/2515-7655/abeab5>
- [16] G. Karagiorgis, C.N. Christodoulou, H. von Storch, G. Tzamalís, K. Deligiannis, D. Hadjipetrou, M. Odysseos, M. Roeb, C. Sattler, Design, development, construction and operation of a novel metal hydride compressor, *Int. J. Hydrog. Energy* 42 (2017) 12364–12374, <https://doi.org/10.1016/j.ijhydene.2017.03.195>
- [17] R. Sharma, E.A. Kumar, A comparative thermodynamic analysis of gas-solid sorption system based on H₂-La_{0.9}Ce_{0.1}Ni₅/LaNi_{4.7}Al_{0.3} and NH₃-NaBr/MnCl₂, *Energy Procedia* 109 (2017) 48–55, <https://doi.org/10.1016/j.egypro.2017.03.047>
- [18] B.S. Sekhar, P. Muthukumar, Performance investigation of a single-stage metal hydride heat transformer, *Int. J. Green. Energy* 13 (2016) 102–109, <https://doi.org/10.1080/15435075.2014.892879>
- [19] Y. Madaria, E. Anil Kumar, Effect of heat transfer enhancement on the performance of metal hydride based hydrogen compressor, *Int. J. Hydrog. Energy* 41 (2016) 3961–3973, <https://doi.org/10.1016/j.ijhydene.2016.01.011>
- [20] A.R.E. Galvis, F. Leardini, J.R. Ares, F. Cuevas, J.F. Fernandez, Experimental behaviour of a three-stage metal hydride hydrogen compressor, *JPhys Energy* 2 (2020), <https://doi.org/10.1088/2515-7655/ab869e>
- [21] X.C. Hu, Z.G. Qi, M. Yang, J.P. Chen, A 38MPa compressor based on metal hydrides, *J. Shanghai Jiaotong Univ* 17 (2012) 53–57, <https://doi.org/10.1007/s12204-012-1229-5>
- [22] X.H. Wang, Y.Y. Bei, X.C. Song, G.H. Fang, S.Q. Li, C.P. Chen, Q.D. Wang, Investigation on high-pressure metal hydride hydrogen compressors, *Int. J. Hydrog. Energy* 32 (2007) 4011–4015, <https://doi.org/10.1016/j.ijhydene.2007.03.002>
- [23] H. Li, X. Wang, Z. Dong, L. Xu, C. Chen, A study on 70 MPa metal hydride hydrogen compressor, *J. Alloy. Compd.* 502 (2010) 503–507, <https://doi.org/10.1016/j.jallcom.2010.04.206>
- [24] V.A. Yartys, M.V. Lototsky, Laves type intermetallic compounds as hydrogen storage materials: a review, *J. Alloy. Compd.* 916 (2022) 165219, <https://doi.org/10.1016/j.jallcom.2022.165219>
- [25] Z. Cao, P. Zhou, X. Xiao, L. Zhan, Z. Jiang, M. Piao, S. Wang, L. Jiang, L. Chen, Studies on Ti-Zr-Cr-Mn-Fe-V based alloys for hydrogen compression under mild thermal conditions of water bath, *J. Alloy. Compd.* 892 (2022) 162145, <https://doi.org/10.1016/j.jallcom.2021.162145>
- [26] Z. Cao, P. Zhou, X. Xiao, L. Zhan, Z. Li, S. Wang, L. Chen, Investigation on Ti-Zr-Cr-Fe-V based alloys for metal hydride hydrogen compressor at moderate working temperatures, *Int. J. Hydrog. Energy* 46 (2021) 21580–21589, <https://doi.org/10.1016/j.ijhydene.2021.03.247>
- [27] Z.M. Cao, P.P. Zhou, X.Z. Xiao, L.J. Zhan, Z.F. Jiang, S.M. Wang, L.J. Jiang, L.X. Chen, Development of Ti_{0.85}Zr_{0.17}(Cr-Mn-V)_{1.3}Fe_{0.7}-based Laves phase alloys for thermal hydrogen compression at mild operating temperatures, *Rare Met* 41 (2022) 2588–2594, <https://doi.org/10.1007/s12598-022-01962-x>
- [28] D.P. Broom, *Hydrogen Storage Materials The Characterisation of their storage properties*, Springer-Verlag, London, 2011.
- [29] M. Dornheim, S. Doppiu, G. Barkhordarian, U. Boesenberg, T. Klassen, O. Gutfleisch, R. Bormann, Hydrogen storage in magnesium-based hydrides and hydride composites, *Scr. Mater.* 56 (2007) 841–846, <https://doi.org/10.1016/j.scriptamat.2007.01.003>
- [30] A. Léon, *Green Energy and Technology Hydrogen Storage*, Springer, 2008.
- [31] M. Latroche, Structural and thermodynamic properties of metallic hydrides used for energy storage, *J. Phys. Chem. Solids* 65 (2004) 517–522, <https://doi.org/10.1016/j.jpcs.2003.08.037>
- [32] D. Duniakov, V. Borzenko, S. Malyshenko, Influence of impurities on hydrogen absorption in a metal hydride reactor, *Int. J. Hydrog. Energy* 37 (2012) 13843–13848, <https://doi.org/10.1016/j.ijhydene.2012.04.078>

- [33] O. Beeri, D. Cohen, Z. Gavra, M.H. Mintz, Sites occupation and thermodynamic properties of the $\text{TiCr}_2\text{-xMnx-H}_2$ ($0 \leq x \leq 1$) system: statistical thermodynamics analysis, *J. Alloy. Compd.* 352 (2003) 111–122, [https://doi.org/10.1016/S0925-8388\(02\)01155-6](https://doi.org/10.1016/S0925-8388(02)01155-6)
- [34] M.T. Hagström, J.P. Vanhanen, P.D. Lund, AB2 metal hydrides for high-pressure and narrow temperature interval applications, *J. Alloy. Compd.* 269 (1998) 288–293, [https://doi.org/10.1016/S0925-8388\(98\)00213-8](https://doi.org/10.1016/S0925-8388(98)00213-8)
- [35] Y. Kojima, Y. Kawai, S. Towata, T. Matsunaga, T. Shinozawa, M. Kimbara, Development of metal hydride with high dissociation pressure, *J. Alloy. Compd.* 419 (2006) 256–261, <https://doi.org/10.1016/j.jallcom.2005.08.078>
- [36] X. Wang, R. Chen, Y. Zhang, C. Chen, Q. Wang, Hydrogen storage alloys for high-pressure suprapure hydrogen compressor, *J. Alloy. Compd.* 420 (2006) 322–325, <https://doi.org/10.1016/j.jallcom.2005.11.001>
- [37] J. Barale, E.M. Dematteis, G. Capurso, B. Neuman, S. Deledda, P. Rizzi, F. Cuevas, M. Baricco, $\text{TiFe}_{0.85}\text{Mn}_{0.05}$ alloy produced at industrial level for a hydrogen storage plant, *Int. J. Hydrog. Energy* 47 (2022) 29866–29880, <https://doi.org/10.1016/j.ijhydene.2022.06.295>
- [38] K.C. Chen, S.M. Allen, J.D. Livingston, Stoichiometry and alloying effects on the phase stability and mechanical properties of TiCr_2 -base laves phase alloys, *Mater. Res. Soc. Symp. - Proc.* 364 (1995) 1401–1406, <https://doi.org/10.1557/proc-364-1401>
- [39] M. Kandavel, V.V. Bhat, A. Rougier, L. Aymard, G. Nazri, J. Tarascon, D.P.J. Verne, Improvement of hydrogen storage properties of the AB2 Laves phase alloys for automotive application, *Int. J. Hydrog. Energy* 33 (2008) 3754–3761, <https://doi.org/10.1016/j.ijhydene.2008.04.042>
- [40] G.U.O. Xiumei, W. Shumao, L.I.U. Xiaopeng, L.I. Zhinian, L.Ü. Fang, M.I. Jing, H.A.O. Lei, Laves phase hydrogen storage alloys for super-high-pressure metal hydride hydrogen compressors, *Rare Met.* 30 (2011) 227–231, <https://doi.org/10.1007/s12598-011-0373-7>
- [41] J.P. Vanhanen, M.T. Hagström, P.D. Lund, Combined hydrogen compressing and heat transforming through metal hydrides, *Int. J. Hydrog. Energy* 24 (1999) 441–448.
- [42] S.S. Bhogilla, H. Niyas, Design of a hydrogen compressor for hydrogen fueling stations, *Int. J. Hydrog. Energy* 44 (2019) 29329–29337, <https://doi.org/10.1016/j.ijhydene.2019.02.171>
- [43] J. Barale, F. Nastro, D. Violi, P. Rizzi, C. Luetto, M. Baricco, A Metal Hydride Compressor for a Small Scale H2 Refuelling Station, *Artic. Submitt. to Appl. Energy.* (2022).
- [44] O. Beeri, D. Cohen, Z. Gavra, J.R. Johnson, M.H. Mintz, Thermodynamic characterization and statistical thermodynamics of the TiCrMn-H_2 (D 2) system, *J. Alloy. Compd.* 299 (2000) 217–226.
- [45] M. Feenstra, G. Özerol, Energy justice as a search light for gender-energy nexus: towards a conceptual framework, *Renew. Sustain. Energy Rev.* 138 (2021) 110668, <https://doi.org/10.1016/j.rser.2020.110668>
- [46] C. Corgnale, M. Sulic, High pressure thermal hydrogen compression employing Ti 1.1 CrMn metal hydride material, *JPhys Energy* 2 (2020) 014003.
- [47] L. Lutterotti, S. Matthies, H.R. Wenk, A.S. Schultz, J.W. Richardson, Combined texture and structure analysis of deformed limestone from time-of-flight neutron diffraction spectra, *J. Appl. Phys.* 81 (1997) 594–600, <https://doi.org/10.1063/1.364220>
- [48] A.R. Galvis E, F. Leardini, J. Bodega, J.R. Ares, J.F. Fernandez, Realistic simulation in a single stage hydrogen compressor based on AB2 alloys, *Int. J. Hydrog. Energy* 41 (2016) 9780–9788, <https://doi.org/10.1016/j.ijhydene.2016.01.125>
- [49] S.V. Alapati, J.K. Johnson, D.S. Sholl, Predicting Reaction Equilibria for Destabilized Metal Hydride Decomposition Reactions for Reversible Hydrogen Storage, (2007) 1584–1591.
- [50] W.S. Tang, P. Raybaud, R. Janot, S. Lracs, U.M.R. Cnrs, U. De Picardie, J. Verne, Enthalpy – entropy compensation effect in hydrogen storage materials: striking example of alkali silanides MSiH_3 (M = K, Rb, Cs), *J. Phys. Chem. C* 118 (2014) 3406–3419, <https://doi.org/10.1021/jp411314w>
- [51] H.M.J. Boots, P.K. De, Bokx, Theory of enthalpy-entropy compensation, *J. Phys. Chem.* 93 (1989) 8240–8243.